

Prospects for the Thomson scattering system on NSTX-Upgrade^{a)}

A. Diallo,^{b)} B. P. LeBlanc, G. Labik, and D. Stevens
Princeton Plasma Physics Laboratory, Princeton, New Jersey 08543-0451, USA

(Presented 7 May 2012; received 6 May 2012; accepted 16 July 2012; published online 7 August 2012)

The paper discusses the projected configuration of the Thomson system on the National Spherical Torus Experiment (NSTX-U). In this paper, we discuss the projected configuration of the Thomson system on NSTX-U. More specifically, we determine, through both optical modeling of the collection optics and in-vessel measurements, that the collecting fibers are to be displaced by at most 1 cm toward the imaging plane along the optical axis. Finally, we estimate the performance of the Thomson system in measuring the electron temperature for NSTX-U discharges. © 2012 American Institute of Physics. [<http://dx.doi.org/10.1063/1.4740267>]

I. INTRODUCTION

A major upgrade of the National Spherical Torus (NSTX) is currently underway. This includes the addition of a second neutral beam heating system, the doubling of the toroidal field, and the doubling of the plasma current, necessitating an increase in the center stack diameter to 62.9 cm (see Menard *et al.*¹). With the upcoming increased NSTX capabilities, the current laser beam path will be obstructed by the new NSTX-U center stack. To avoid such obstruction, significant efforts have been underway to re-aim the laser beams, assess the collection optic capabilities, install a beam dump in vessel, and project the electron temperature resolution in future NSTX-U discharges.

II. CONFIGURATION OF THE THOMSON SCATTERING SYSTEM

The NSTX Thomson system^{2,3} consists of two 1.6-J 30 Hz Nd:YAG lasers with pulse widths of 8 ns, 42 radial channels (see Ref. 3 for a detailed description), a large collection optic, and a beam dump. Each radial channel consists of a four- or six-wavelength band polychromator (design adapted from Carlstrom⁴) collecting the scattered photons. This system has been operational on NSTX for many years and routinely provided valuable electron temperature, density, and pressure profiles, as well as line-integrated densities.^{2,5} Figure 1 depicts a midplane cross section of NSTX-U, where the center stack diameter has been doubled. The new center stack is shown to obstruct the current laser beam path. The laser beams are re-aimed and a new ex-vessel in vacuum beam dump is added. In addition, the new nominal laser beam path (midpoint between the two laser centers) clears the NSTX-U center stack by 8.0 cm.

The impact of this beam shift on the photon collections is analyzed using the OSLO (Ref. 6) code. Figure 2 depicts both NSTX and NSTX-U beam paths, with their associated rays. As shown in this figure, the ray tracing is optimized to obtain

a focused image at the location of the NSTX-U laser beam path. Note that the Multi-Point Thomson Scattering (MPTS) collection optic consists of an aperture stop, a large polarizer (located near the aperture stop shown in Fig. 2(b)), a spherical mirror with a radius of curvature of 68 cm, and arrays of fiber bundles. In this modeling, only the fiber holder was rotated ($<0.9^\circ$) and translated to obtain the best focus on the NSTX-U beam path. In this optimization, we elected to preserve the spatial point in the far edge i.e., $R = 1.57$ cm (see Fig. 2), which was routinely used to diagnose electron density and temperature in front of the high harmonic fast wave antenna.

Figure 3 shows an example of studies of the root-mean-squared (rms) spot size at the fiber bundle as a function of the fractional object height along the laser beam. The individual fiber size is around $535 \mu\text{m}$, which yields a fiber bundle height of 1.59 mm. This figure shows similar rms spot size as for both the NSTX and NSTX-U configurations. Note that the optimum focus is obtained when the fiber holder is displaced by about 1.7 cm as displayed in Figure 2(b). While this tuning represents the optimum motion of the fiber bundle holder required to achieve a good focus at the NSTX-U beam path, we are also contemplating displacement (rotation around the vertical axis and translation) of the whole optics box. This optical box displacement could yield greater flexibility during the

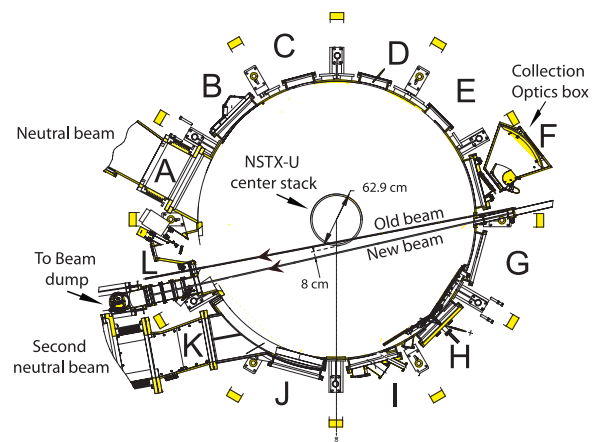


FIG. 1. NSTX-U midplane cross section shows the new laser beam path next to the old path, and the collection optics (at bay F).

^{a)}Contributed paper, published as part of the Proceedings of the 19th Topical Conference on High-Temperature Plasma Diagnostics, Monterey, California, May 2012.

^{b)}Email address: adiallo@pppl.gov.

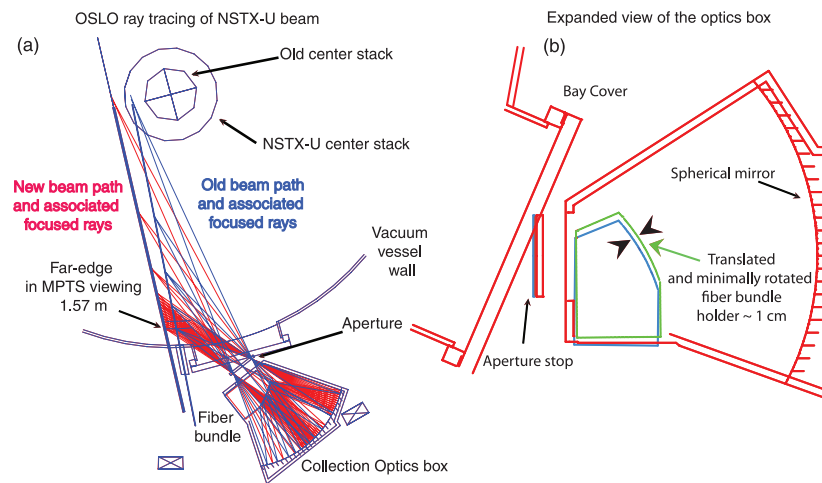


FIG. 2. (a) Ray tracing using OSLO showing both the old and new laser beam paths. (b) Close-up on the optics box depicting the displaced fiber holder associated with rays in (a).

alignment procedure of the MPTS system. Using ray tracing tools, we showed that in order to preserve the MPTS system capabilities on NSTX-U, the fiber bundle holder in the collection optic box is required to be minimally adjusted ($\sim 1\text{--}2$ cm motion), as shown in Fig. 2(b). This range of displacement was also confirmed during in-vessel measurements.

In addition, efforts are underway to design an in-air laser beam dump which would be located 10.6 m from the vessel exit at bay L (see Figure 1). This beam dump is composed of two infrared absorbing glass plates. The first glass is oriented at Brewster's angle and the relative angle between the two glasses is set to be around 5° to achieve an optimum number of bounces of the laser beams. Note that each bounce results in a laser beam absorption.

III. ASSESSMENT OF NSTX-U THOMSON SCATTERING SYSTEM PERFORMANCE

A. Electron temperature resolution

The MPTS system consists of 42 radial channels (12 of which have been newly implemented and are discussed in Ref. 3). Each radial channel is represented by a polychroma-

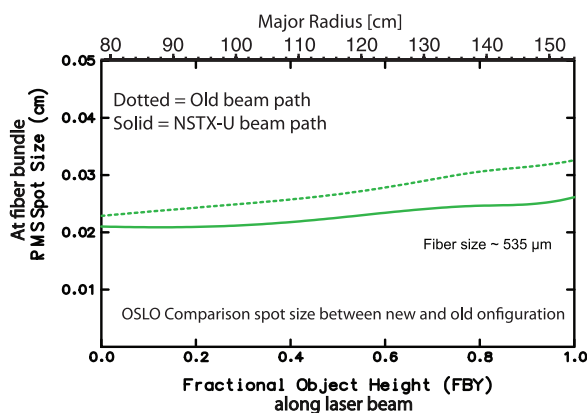


FIG. 3. Shown here is a comparison of the image rms size at the fiber holder for the two configurations (NSTX and NSTX-U). The resolution is better than a fiber diameter ($535\ \mu\text{m}$).

tor, which measures the Thomson scattered spectrum. In the current configuration, each polychromator consists of either 4 or 6 wavelength bands. Figure 4 shows an example of the polychromator's quantum efficiency weighted transmission curve with examples of overlaid computed Thomson spectra.

The measured scattered spectra from the polychromators are then fitted to yield both electron density and temperature. NSTX-U is expected to operate at high electron temperatures (~ 10 keV) during high harmonic fast wave heating¹ and at temperatures up to 2 keV for beam heated H-mode plasmas. In the analysis below, the high harmonic fast wave heating (HHFW) discharges are all low density shots ($\times 3$ range). In the beam-heated discharges, however, there is a much larger range of accessible densities ($\times 12$ range). Given the wide range of expected temperatures, we both extrapolate and forward-model the temperature relative errors to be expected on NSTX-U for HHFW discharges. The extrapolation is constrained by the available data, which spans high and low density regimes. The low density regime occurs at high temperatures for both types of polychromators, which makes the statistical contribution to error in T_e the same between the two polychromators. We found that the density has little effect on the trends shown in Figure 5. The remaining contribution to the error in T_e is discussed below.

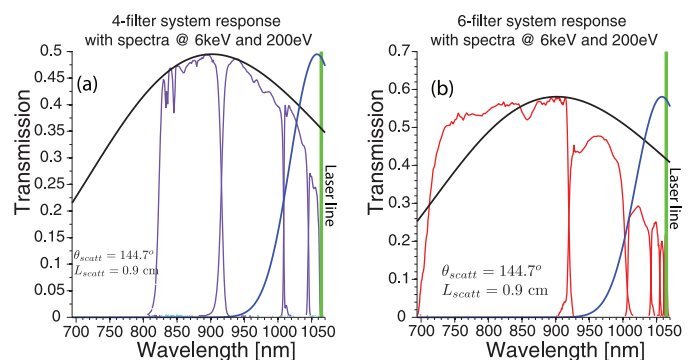


FIG. 4. Transmission curves (folding in the detector quantum efficiency) with examples of the computed Thomson scattered spectra at 6 keV and 200 eV (see Ref. 7).

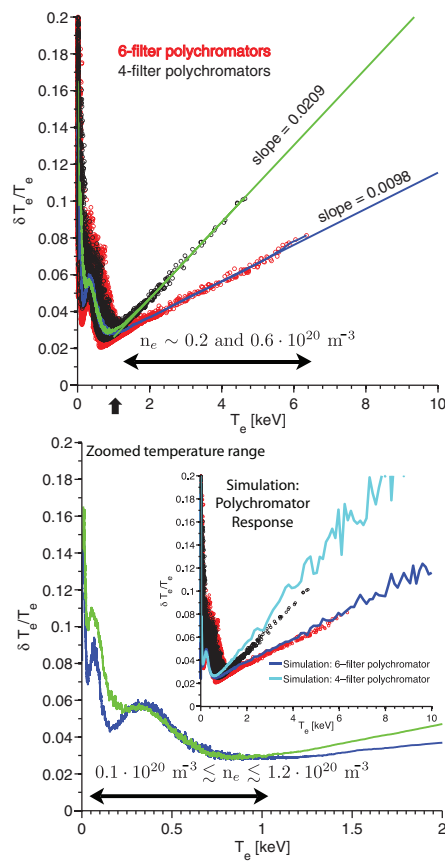


FIG. 5. (Top) Electron temperature relative error as a function of measured temperature for both neutral beam heated and high harmonic fast wave heated discharges. Comparison between 4- and 6-filter polychromators. (Bottom) Close-up look at the low temperature range. Note the corresponding densities are also included in the plots. The inset represents the simulated polychromator response with the actual experimental data overlaid.

Figure 5 depicts a variation of $\delta T_e/T_e$ as a function of T_e for the two types of polychromators in the MPTS system using previous NSTX discharges (both neutral beam-heated and high harmonic fast wave-heated). The 4-wavelength-band polychromator shows larger error ($\delta T_e/T_e$) compared to the 6-wavelength-band polychromator for electron temperatures exceeding 1 keV (as indicated with an arrow in Figure 5). Extrapolation of this scaling at electron temperatures expected on NSTX-U suggests that expected errors on the electron temperature measurements should be $\sim 11\%$ for the 6-wavelength-band polychromator and $\sim 20\%$ for the 4-wavelength-band polychromator. Note that the main difference between the two sets of polychromators is that the 4-wavelength polychromator under-samples the electron distribution tail (see Figure 4(a)).

At temperatures below 250 eV, the 4-wavelength polychromator instrument response yields errors larger than the 6-wavelength band polychromator (see bottom plot of Figure 5). This difference could be attributed to the inferior spectral resolution near the laser wavelength in the 4-filter polychromator. For temperatures ranging between 250 eV and 1 keV, the two types of polychromators show similar errors (see bottom plot in Figure 5). In regions where $T_e \geq 1\text{keV}$, the 6-filter polychromator performs better than the 4-filter polychromator system.

Using forward modeling, where scattered spectra were run through our analysis routines, we generate the expected temperature error estimates for the two types of polychromators as shown in the inset of Figure 5. Here the density is assumed fixed. This figure shows agreement throughout the temperature range measured and confirms the linear trend previously extrapolated (for $T_e > 6\text{keV}$) from the data. Proper filter arrangements for improved temperature resolution, both in the core and edge, will be the subject of future publications.

B. NSTX-U discharge length implications and future work

NSTX-U is expected to operate with 5-s discharges, which will likely cause coating of the vacuum interface windows and modify the overall window transmission. In the current setup, great care has been taken to routinely perform window calibrations to monitor potential drops in transmission. The calibration consists of an illuminating probe inserted in the vacuum side that enables us to determine the chromatic transmission drop due to window coatings during the experimental campaign. While this approach has been successful in NSTX discharge length ($< 1\text{s}$), an improvement of this illuminating probe is under investigation to allow for in-between discharge calibration.

The projected increased NSTX-U capabilities in combination with long discharge lengths ($\sim 5\text{s}$), will increase the background light due to impurity radiations. Past experience with shorter discharge lengths (about 1s) have shown impurity radiation swamping the wideband filter detector, rendering the tail of the distribution data unusable due to saturation. To avoid such issues, we are currently investigating means to control the overall background light responsible for such saturation. The planned approach includes (i) the addition of a second rotatable polarizer to reduce the light intensity (note that the current system includes a polarizer to select the Thomson scattered light), (ii) dynamically reducing the detector gain associated with the wideband filter, and (iii) reducing the wideband filter bandwidth resulting in less collected light, in combination with an increase of filter numbers and hence of the number of polychromator channels to conserve the spectral resolution. The second rotatable polarizer is an alternative to the current setup where partial shuttering is used. In fact, the second polarizer can potentially offer a uniform overall reduction of the light intensity throughout the field of view.

ACKNOWLEDGMENTS

A.D. thanks S. Gerhardt and H. Yuh for providing a list of some relevant H-mode shot numbers, and M. Podesta for reading the paper. Work supported by U.S. Department of Energy (DOE) Contract No. DE-AC02-09CH11466.

¹J. Menard *et al.*, *Nucl. Fusion* **52**, 083015 (2012).

²B. P. LeBlanc *et al.*, *Rev. Sci. Instrum.* **74**, 1659 (2003).

³B. LeBlanc *et al.*, "Radial Resolution Enhancement of the NSTX Thomson Scattering Diagnostic," *Rev. Sci. Instrum.* (these proceedings).

⁴T. Carlstrom, *Rev. Sci. Instrum.* **72**, 2855 (2001).

⁵D. Johnson *et al.*, *Rev. Sci. Instrum.* **70**, 776 (1999).

⁶See <http://lambdare.com> for Oslo lambda research corporation.

⁷A. Selden, *Phys. Lett. A* **79**, 405 (1980).